Nano Energy (2016) 20, 283–293

Available online at www.sciencedirect.com

ScienceDirect

journal homepage: www.elsevier.com/locate/nanoenergy

COMMUNICATION

Force-assembled triboelectric nanogenerator with high-humidity-resistant electricity generation using hierarchical surface morphology

Dongjin Jang[a,1], Younghoon Kim[a,1], Tae Yun Kim[b], Kunsuk Koh[c], Unyong Jeong[c,*], Jinhan Cho[a,*]

[a]*Department of Chemical and Biological Engineering, Korea University, Seoul 136-713, Republic of Korea*
[b]*School of Advanced Materials Science and Engineering, Sungkyunkwan University (SKKU), Suwon 440-746, Republic of Korea*
[c]*Department of Materials Science and Engineering, Pohang University of Science and Technology, Pohang, Gyungbuk 790-784, Republic of Korea*

Received 30 September 2015; received in revised form 14 December 2015; accepted 22 December 2015
Available online 31 December 2015

KEYWORDS
Triboelectric nanogenerator;
Force-assembly;
Colloids;
Dual-sized structures;
Humidity

Abstract
We introduce a novel, robust, cost-effective, and scalable approach for the preparation of a large-area force-assembled triboelectric nanogenerator (FTENG), which allows a stable and high electric output under a wide range of humidity conditions through its dual-sized morphology (i.e., microstructures and nanostructures). In this study, hexagonally packed colloidal arrays prepared by a force assembly approach rather than by conventional self-assembly were used as a mold for a triboelectric poly(dimethylsiloxane) (PDMS) replica with desired pattern shapes (intaglio and embossed structures) and sizes. The morphological size of the PDMS films was determined by the diameter of the force-assembled colloids. The electrical output performance of FTENGs composed of electrodes and a PDMS film increased substantially as the size of the micropores (for intaglio-structured PDMS) or embossed features (for embossed-structured PDMS) decreased. Furthermore, the triboelectric PDMS film with micro-/nanosized features (i.e., dual-embossed PDMS) displayed a remarkable electrical output of 207 V (open-circuit voltage under a compressive force of 90 N in relative humidity (RH) of 20%) and high hydrophobicity compared to that of PDMS films with flat, intaglio or embossed structures. This device maintained a high electric output even in a high-humidity environment (i.e., open-circuit output voltage ~175 V in RH 80%). Our approach using force-assembly and

*Corresponding authors.
E-mail addresses: ujeong@postech.ac.kr (U. Jeong), jinhan71@korea.ac.kr (J. Cho).
[1]These authors equally contribute to this work.

http://dx.doi.org/10.1016/j.nanoen.2015.12.021

hierarchical surface morphology will provide a novel and effective framework for developing strong power sources in various self-powered electronics.

Introduction

Since the beginning of this century, the rapid expansion and evolution of the use of various wireless electronics has increasingly required sustainable, renewable and maintenance-free energy sources. Self-power generation is possible with these energy sources, which is in accordance with modern society's need to cope with both ecological concerns and the decreasing availability of fossil fuels [1-6]. Among the various types of self-power generators, including those that use light, heat and mechanical force, triboelectric nanogenerators (TENGs) have recently been considered as a notable alternative for energy production and a renewable resource in green nanotechnology. TENGs can effectively convert mechanical energy, which is readily available from a variety of irregular sources that exist in our daily lives and surroundings, into sustainable electrical energy with high energy conversion efficiency, good scalability and facile fabrication [7-12].

These devices are designed to use generated triboelectricity as the charge-driving source for electric current generation. When the surfaces of good electron donor and acceptor materials undergo periodic contact and separation, the generation and transfer of electrostatic charges cause a potential difference across electrodes; this potential difference can drive the flow of electrons through an external circuit. Although many studies have sought to improve the electrical performance of TENGs, their main focus has been the selection of triboelectric materials and the switching approaches for periodic contact/separation [11,13-23]. Recently, much attention has been paid to frictional electrification, performance stability of devices in humid environments [24-28], and control of the surface morphology, which has a critical effect on charge generation and electric output. For example, Nguyen and Yang reported that the generated charges of TENGs, which were based on pyramid-patterned PDMS and Al electrode, increased more than 20% when relative humidity (RH) decreased from 90 to 10% [27]. Additionally, Lee et al reported that the electric output voltage of sponge structure-based TENGs decreased from approximately 130 to 108 V with increasing RH from 20 to 80% [11]. In view of pattern shape-related performance, micropatterned TENGs prepared using Si-mold-based photolithography [29] and an electrodeposition process [8] have been reported to improve electrical performance as a result of an increase in the contact area between two different triboelectric plates compared with the performance of a natural flat surface. Several research groups have reported that high-performance TENGs can also be achieved by triboelectric films with unique nanostructures that were prepared by a variety of self-assembly processes (e.g., selective etching of spontaneous block copolymer templates [12] or nanoparticle self-assembly [22,30]). However, in many cases, the creation of such micro- or nanostructures on triboelectric materials requires relatively complex and delicate processing over a small-scale area. When applied to large-area TENGs, these techniques often pose considerable difficulty in delivering practical and reproducible design structures with high mechanical stability. Additionally, their output performance is vulnerable to highly humid environments. From this perspective, achieving a high degree of control over the size scalability, good fabrication efficiency, high mechanical robustness of morphological features, and humidity-resistant electrical output is a challenging obstacle to the realization of high-performance TENGs.

Here, we introduce a TENG with good electrical performance, remarkable humidity-resistant properties, and mechanically stable dual-sized structures (i.e, micro/nanostructures) over a large scale, which were created using a force-assembly method based on mechanical rubbing and imitating the morphological uniqueness (i.e., dual-sized structures) of a superhydrophobic surface with water repellency. In particular, our approach is advantageous to the preparation of a large-area TENG because the mechanical rubbing process is not restricted by substrate size. In our study, hexagonally close-packed colloid-coated substrates were used as a mold for the preparation of triboelectric plates with intaglio and embossed micro/nanostructures. The electrical performance of force-assembled TENGs (i.e., FTENGs), which strongly depends on the contact surface area and the morphological features, was easily controlled by the proper diameter selection of mechanically rubbed colloids. We also highlight that triboelectric poly(dimethylsiloxane) (PDMS) films with embossed micro-/nanostructured features (i.e., dual-embossed PDMS) can maintain a high level of electrical output over a wide range of humidity conditions (207 V at 20% relative humidity (RH) and 174 V at 80% RH) because of their enhanced hydrophobic properties. Furthermore, the performances of the dual-embossed PDMS films were maintained without electrical degradation during long-term cycling and time, which is attributed to the embossed features having two different sizes fused into an all-in-one PDMS. This approach can provide a simple and cost-effective tool for the fabrication of large-area triboelectric nanogenerators with highly humidity-resistant performance, irrespective of the substrate size and shape.

Experimental section

Materials

Dimethylsiloxane, PDMS (Sylgard 184) and PS colloids with diameters of 0.6, 1, 2, and 5 μm were purchased from

Sigma-Aldrich, Dow Corning and Microparticles GmbH, respectively.

Preparation of colloidal monolayer-coated substrates

The PDMS prepolymer and cross-linker agent were mixed in a weight ratio of 10:1 and then mechanically stirred for 30 min. The bubbles formed from PDMS prepolymer mixture were removed in the vacuum chamber for one day. After such a process, the mixture was spin-coated at 3000 rpm for 30 s onto a Si wafer, and the formed PDMS-coated substrates were then cured at 80 °C for 5 h. After the curing process, dry powder of a negatively charged PS colloids with a diameter of 1, 2, or 5 μm was placed onto the PDMS-coated Si wafer and then mechanically rubbed with the other PDMS-coated substrate. This force-assembly process transferred the respective colloids to the PDMS-coated substrates, resulting in the formation of hexagonally packed colloidal arrays.

Preparation of triboelectric PDMS replica

For preparing the well-controlled PDMS films, we have used doctor-blade process after pouring the PDMS prepolymer mixture (PDMS prepolymer: cross-linker agent = 10:1, w/w) into PS colloidal monolayer-coated PDMS template. The thickness of mold used for doctor blade was approximately 500 μm. Therefore, the total thickness of the resultant PDMS films prepared from doctor blade approach was fixed at approximately 500 μm. After such a process, these films were thermally cured at 150 °C for 40 min. The cured PDMS film was carefully peeled from the PDMS template and then soaked in acetone for 24 h to completely remove the residual PS colloids adsorbed onto the surface of the detached PDMS films. After this etching process, the triboelectric PDMS replica with the intaglio (or microporous) structure, which was referred to as intaglio-PDMS, was obtained. In this case, the size of the micropores was determined by the diameter of the mechanically rubbed colloids. A triboelectric PDMS replica with an embossing structure (i.e., embossing-PDMS film) was prepared using an intaglio-PDMS replica instead of hexagonally packed PS colloid-coated substrates. First, trichloro (1*H*,1*H*, 2*H*, 2*H*-perfluorooctyl)silane was coated onto the intaglio-PDMS template, and the PDMS prepolymer mixture was subsequently poured onto the template surface (this surface treatment allows the facile detachment of the embossing-PDMS replica from the intaglio-PDMS template). After this step, all experimental procedures, including the curing, film detachment, etching, and drying processes, for embossed-PDMS were identical to those for intaglio-PDMS.

Preparation of triboelectric PDMS with dual-embossed structure

For the preparation of dual-embossed PDMS with micro/nanostructures, cationic PEI was electrostatically adsorbed onto the anionic PS colloid (diameter ~2 μm)-coated substrates; anionic PS colloids (concentration of PS colloidal solution ~1 wt%) with a diameter of approximately 607 nm were then additionally deposited onto PEI-coated substrates in aqueous solvent. The formed substrates were dipped into water for 5 min to remove the weakly adsorbed PS colloids and then dried under vacuum for 2 h. Furthermore, these substrates were chemically treated with trichloro (1*H*,1*H*, 2*H*, 2*H*-perfluorooctyl) silane to form the hydrophobic surface. A dual-embossed-PDMS replica was obtained from the successive replica of the dual-sized PS colloid-coated substrate using the aforementioned experimental procedures.

Measurements

Surface morphologies of intaglio-, embossed-, and dual-embossed-PDMS were investigated by field-emission scanning electron microscopy (FE-SEM) (Hitachi Inc., model S-4800). A pushing tester (Labworks, Inc., model ET-126-1) was used to produce a vertical compressive strain in the FTENGs with a distance of 450 μm between the Al top (with 63 μm thickness) and bottom electrodes and a contact area of $1.5 \times 1.5\ cm^2$. A Tektronix DMO 3052 digital phosphor oscilloscope and a low-noise current preamplifier (Stanford Research Systems, Inc., model SR570) were used for open-circuit output voltage and short-circuit output current, respectively. Additionally, water contact angle measurement was performed using Phoenix-300 (Surface Electro Optics Co., Ltd.). In this case, the volume of water droplet was approximately 11 μL. Additionally, potential distribution of flat-, embossed-, and dual embossed-PDMS devices was investigated using COMSOL multiphysics software.

Results and discussion

For the preparation of triboelectric PDMS films with differently shaped patterns (i.e., intaglio and embossed structures) and various sizes (Scheme 1), dry powdered polystyrene (PS) (or silica) colloids with a diameter of 1, 2, or 5 μm were first mechanically rubbed against a rubbery material, i.e., the PDMS-coated substrates, using another rubbery substrate. This rubbing process transferred the respective colloids to the rubbery substrates [31-33]. After being rubbed for 10 s, the PS colloids were force-assembled into hexagonally close-packed monolayers on the surfaces of both rubbery substrates (Figure S1), which were then used as a mold for triboelectric PDMS films with an intaglio microstructure. Notably, the hexagonal packing structure of colloids with a defined diameter can maximize the triboelectric surface area of a PDMS replica that is closely related to the amount of charge generation.

In this case, the triboelectric PDMS film replicated from the PS monolayer-coated substrate displayed intaglio patterns with a nearly perfect hexagonal structure over a 4-in wafer and without any residual PS colloids (Figure 1a). The micropore sizes of intaglio-structured PDMS (intaglio-PDMS) films that were replicated from 1, 2, and 5 μm-sized PS colloids were slightly decreased to approximately 0.9, 1.9, and 4.8 μm, respectively, because of the shrinkage of cross-linked PDMS. An intaglio-PDMS film was used as a replica mold for the preparation of the embossed microstructured PDMS (embossed-PDMS) films. Similarly, the bump sizes of the resultant embossed-PDMS films were further decreased to

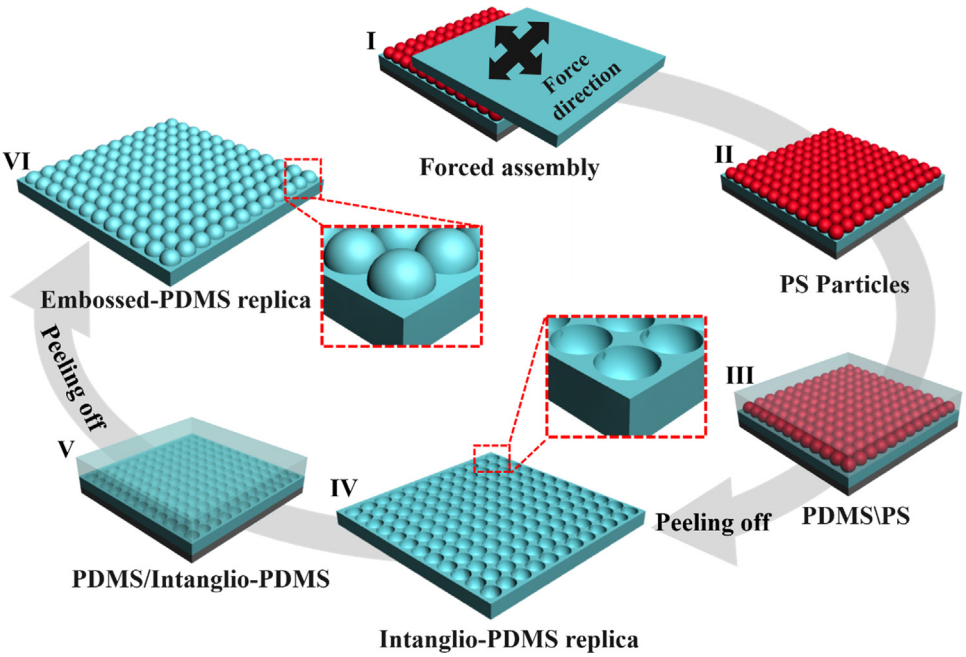

Scheme 1 Schematic showing the preparation of the intaglio- and embossing-patterned PDMS films. The PDMS films with intaglio (IV) and embossing patterns (VI) were prepared from a replica of a PS colloid monolayer-coated substrate (II) and intaglio-PDMS substrate (IV), respectively.

approximately 0.8 (by 1 μm PS colloids), 1.8 (by 2 μm PS colloids), and 4.6 μm (by 5 μm PS colloids) (Figure 1b). As a result, large-area triboelectric PDMS films with size-controllable morphological features and nearly perfect spatial registration were easily prepared (see Experimental Section). Although we demonstrated the wafer-scale replica of intaglio- and embossed-PDMS films, the size of patterned PDMS films obtained using force assembly is limited only by the size of the substrate, and this technique can be further scaled.

Figure 2a presents a schematic of the fabrication of FTENGs. The FTENG was composed of an Al plate and a replicated PDMS film, two components with a large difference in their abilities to lose and gain electrons, as shown in the well-known triboelectric series [17]. In this case, the Al plate was used as a contact electrode and as a triboelectric material with positive polarity. A polyacrylate film was glued to one side of the replicated PDMS film, with negative triboelectric polarity, and an additional Al electrode (bottom) was subsequently attached to the opposite side of the polyacrylate. For the effective contact/separation of the triboelectric plates (i.e., the Al electrode and PDMS film), four springs were attached to the corners of the substrates, which left a narrow space between the plates [22] (see Supporting Information, Figure S2). Furthermore, to investigate the electrical output of FTENGs with various contact surface areas, we prepared a variety of FTENGs with features of different morphologies and sizes (i.e., intaglio- and embossed-FTENGs) and a TENG with flat triboelectric plates: (I) flat TENG (i.e., flat Al/flat PDMS film), (II) intaglio-FTENGs [i.e., flat Al/intaglio-PDMS with different micropore sizes (0.9, 1.9, and 4.8 μm)], and (III) embossed-FTENGs [i.e., flat Al/embossed-PDMS with different embossed feature sizes (0.8, 1.8, and 4.6 μm)].

Figure 2b and c display the electrical output generated by a flat TENG and an intaglio-FTENG replicated from 5 μm PS colloidal arrays (designated as "5 μm-intaglio-FTENG") under a repeated compressive force of 70 N at an applied frequency of 5 Hz with 20% RH. In the case of the flat TENG, the electrical output was approximately 57 V and 33 mA m^{-2}. However, under the same mechanical force, the 5 μm-intaglio-FTENGs displayed an output voltage and current density of approximately 103 V and 48 mA m^{-2}, respectively. In addition, polarity-switching tests revealed that the output voltage and current of 5 μm-intaglio-FTENG originated from the periodic contact/separation between the contact electrode and PDMS and not the measurement system (see Supporting Information, Figure S3). This electrical energy generation can be generally explained by the coupling between the triboelectric effect and electrostatic induction [22,34]. More specifically, when two triboelectric plates (i.e., contact electrode and PDMS film) with separation distance (d_0) at the initial state are brought into surface contact by an external compressive force, electrons are injected from the contact electrode with high electron-donating character and are then transferred to the PDMS film with high electron-retaining character, resulting in surface triboelectric charges (see Supporting Information, Figure S4). However, as the separation distance approaches d_0 again by the release of the compressed springs, the separated charges generate an electric field oriented from the back electrode to the contact electrode, thereby inducing a greater potential at the contact electrode. This potential difference causes an electron flow from the back Al electrode to the contact Al electrode, thus inducing a potential drop that eliminates the tribocharge-induced potential. When the gap between the triboelectric plates returns to the initial distance (d_0), the positive triboelectric charges on the contact Al electrode are fully screened, inducing the same amount of positive charges on the back Al electrode. However, when the separation distance is sequentially decreased again by compressive

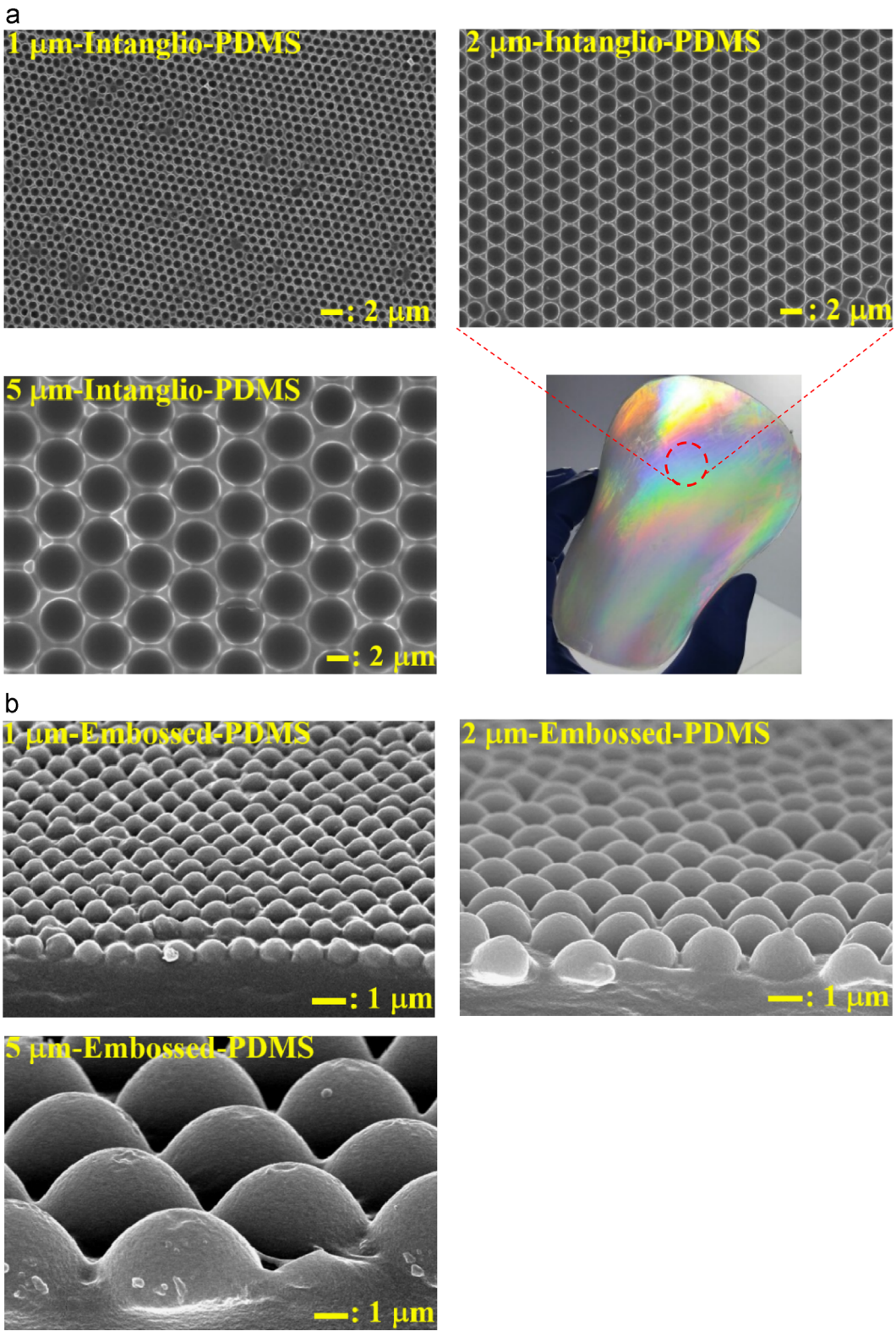

Figure 1 (a) Photographic and SEM images of intaglio-PDMS films replicated from 1, 2, and 5 μm-PS monolayer-coated Si wafer. (b) Tilted cross-sectional SEM images of embossed-PDMS films.

force, the electric potential difference with reversed polarity is re-established, inducing the back-flow of electrons (i.e., negative current) to neutralize the positive triboelectric charges in the bottom Al electrode.

On the basis of this energy generation mechanism, the improved electric output of the 5 μm intaglio-FTENG implies that a microporous PDMS film with a large surface area can generate a larger amount of triboelectric charge than a flat

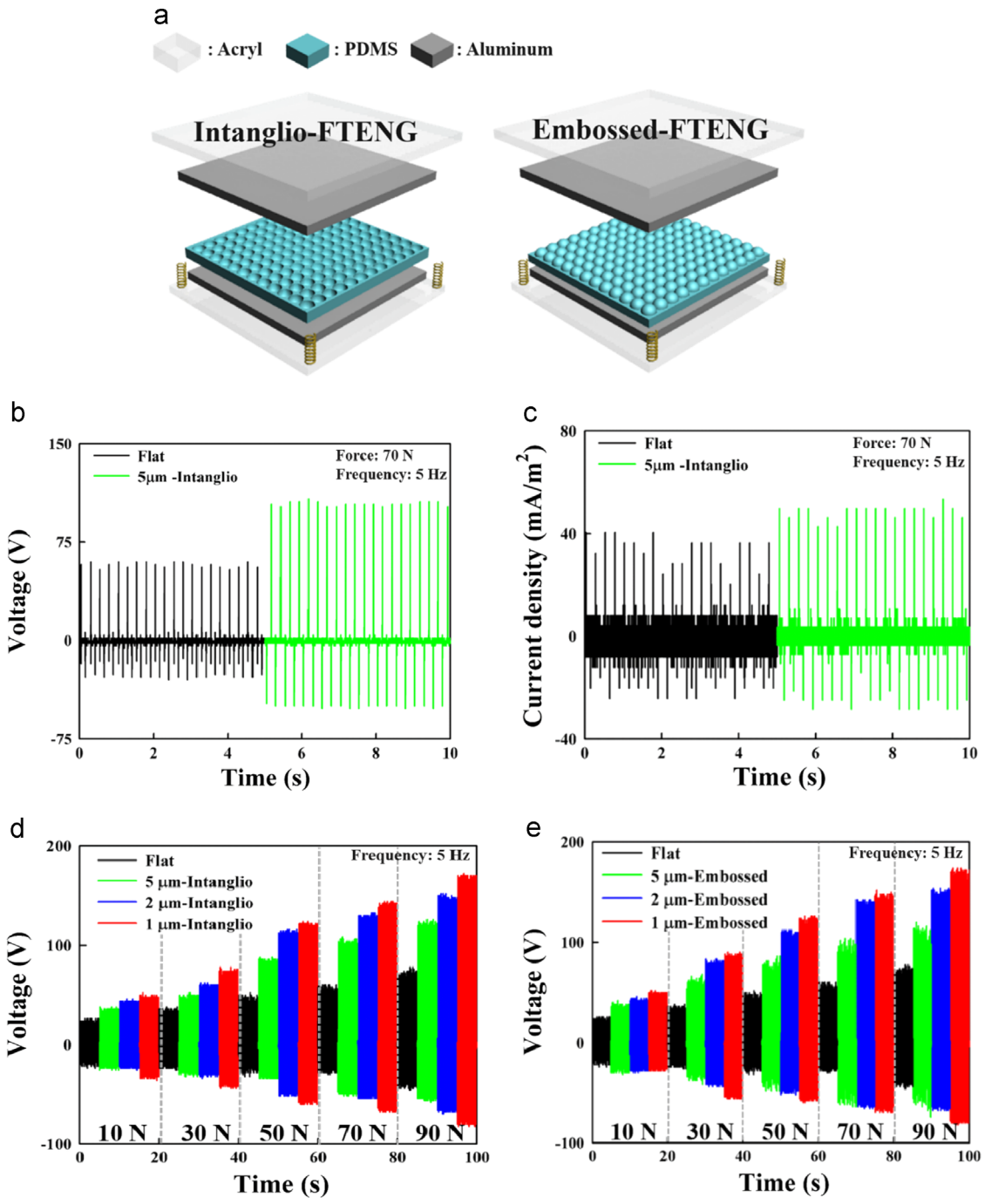

Figure 2 (a) Schematic showing the structure of FTENG based on the intaglio- and embossed-PDMS films. (b) Output voltage and (c) current density of a flat TENG and a 5 μm-intaglio-FTENG. Changes in the output voltage of (d) intaglio-FTENGs with a different micropore size and (e) embossed-FTENGs with a different embossing feature size as a function of the applied compressive force.

PDMS (flat TENG) film under the same mechanical force. Although the porous structure can prevent intimate contact between the electrode and PDMS plate under low compressive force, greater compressive force can cause the microporous and elastic PDMS film to be readily deformed, thus providing a larger contact area between the two plates. In addition to the increased contact area, electrostatic induction may contribute to the generation of triboelectric charges in the regions of noncontact. Lee et al. have recently reported that a PDMS film with a sponge-type microstructure generated additional triboelectric charges on the surface of the inner pores by electrostatic induction, as well as a notable capacitance change, under compressive force. The resultant TENGs that were based on a microstructured PDMS induced an enhanced electrical output compared to the flat-film-based TENG [11].

To further improve the electrical output of FTENGs, we systematically investigated the change in the output voltage

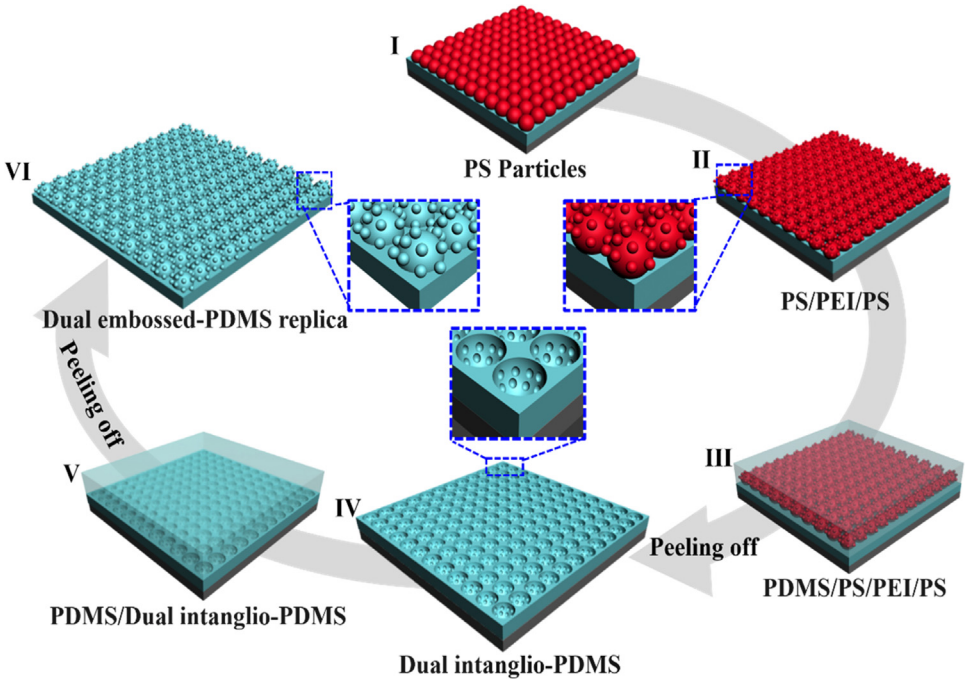

Scheme 2 Schematic showing the preparation of dual-embossed-PDMS films.

and current density of FTENGs according to the micropore size of the PDMS film and the applied compressive force (Figures 2d and S5a). As the micropore size was decreased to approximately 0.9 μm (from 1 μm intaglio-FTENG) and the compressive force was increased from 10 to 90 N, the output voltage (i.e., open-circuit voltage) and current density (i.e., short-circuit current density) increased considerably to 170 V and 103 mA m^{-2}, respectively. This good electrical performance was also observed in the embossed-PDMS replicated from intaglio-PDMS films (Figures 2e and S5b). In particular, as the size of the embossed features decreased from 4.6 (for 5 μm embossed-FTENG) to 0.8 μm (for 1 μm embossed-FTENG) and as the compressive force increased from 10 to 90 N, the output voltage and current were approximately 171 V and 104 mA m^{-2}, respectively, which are nearly identical to those measured from the corresponding 1 μm intaglio-TENG. These results imply that triboelectric PDMS films can display a similar electrical output only if they have a comparable increase in surface area under the same compressive force.

To further increase the contact surface area (also including air voids) and hydrophobic character for high-performance FTENGs, nanosized PDMS protuberances were introduced into the embossed microstructured PDMS films with the aid of electrostatic self-assembly (Scheme 2). These features bear a striking likeness to superhydrophobic surfaces that exhibit low surface energy and hierarchical surface roughness on a dual-length scale [35–40]. An FE-SEM image of micro-/nanosized PDMS protuberances (dual-embossed structure) are shown in Figure 3a. In this case, anionic PS colloids with a diameter of approximately 600 nm were electrostatically adsorbed onto a cationic poly(ethylene imine) (PEI) layer, which coated a force-assembly-generated array of hexagonally packed 2 μm PS colloidal particles (see Experimental Section). After the deposition of the 600 nm-sized PS colloids, a subsequent PDMS replica of this array produced an embossed PDMS film with dual-sized morphological features (i.e., an embossed feature size of approximately 1.8 μm and protruding nanostructures approximately 450 nm in size) [32–34]. These dual-embossed PDMS films were mechanically stable under a cycled compressive force because the embossed features with two different sizes were fused into an all-in-one PDMS. The output voltage and current density of a dual-embossed-FTENG under a compressive force of 90 N were approximately 207 V and 141 mA m^2, respectively, which are higher than those for the embossed-FTENGs without nanosized protuberances (Figure 3b and c). This electrical performance remained stable over approximately 18,000 cycles at 5 Hz, and additionally was maintained after 5 weeks (Figures 3d and S6).

Additionally, resistors were connected as external loads to examine the effective power of dual-embossed-FTENG (Figure 3e). With increasing load resistance under the force of 90 N, the instantaneous voltage peak increased, and on the other hand current peak density dropped because of ohmic loss. As a result, the instantaneous power output reached the maximum value (i.e., $W=I^2_{peak}\ R=5.42\ W/m^2$) at an external load resistance of 10 MΩ (Figure 3f). Therefore, FTENG can be equivalent to be considered as a current source with a large internal resistance when the external resistance load was significantly smaller than the internal resistance [41].

Furthermore, we investigated the effect of dual-sized features on the triboelectric potential of dual embossed-PDMS device through analytical simulations using COMSOL multiphysics software (Figure 4a). For the convenience of simulation, the Al top plate with the width of 30 μm and thickness of 10 μm was placed above the PDMS film with the same dimensions with Al top electrode. The distance between PDMS and Al electrode was fixed at 20 μm, and additionally the force was not applied in our simulation. A triboelectric charge

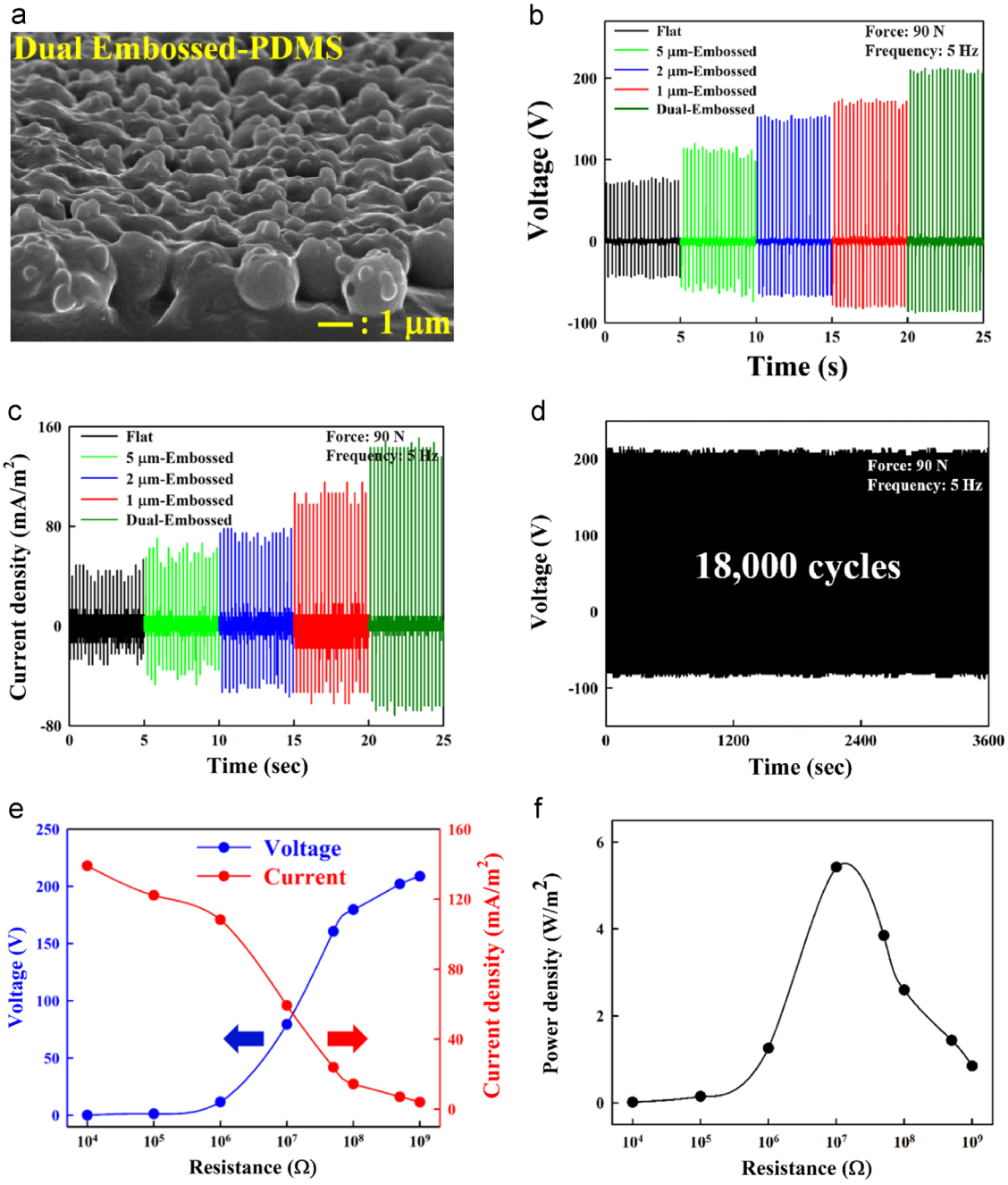

Figure 3 (a) FE-SEM image of dual-embossed-PDMS films. (b) Total output voltages and (c) current densities of a flat TENG, 1 μm- and 2 μm-embossed-FTENGs and a dual-embossed-FTENG. (d) Electrical stability tests of the dual embossed-FTENG at 20% RH. (e) Dependence of the peak voltage and peak current density on external load resistance under the compressive force of 90 N. (f) Dependence of the instantaneous power output on external load resistance under the compressive force of 90 N.

density of two tribo-charged surfaces were assigned with $\pm 32.3\ \mu C/m^2$. In these cases, the triboelectric potential of the dual embossed-PDMS film notably increased when the contact area was increased, implying the generation of greater charge density on its surface compared to those on the surfaces of flat- and embossed-PDMS films. Given that an increase of triboelectric charge density is directly related to an increase in transferred charges and to a greater triboelectric potential difference between the electrodes [8,42], the remarkable electrical performance of the dual-embossed-FTENG is closely related to the formation of dual-sized PDMS features.

Furthermore, we examined the influence of the surface-morphology-induced hydrophobicity on the electrical performance of FTENGs in a humid environment. Water droplets placed onto flat PDMS, 1 μm embossed-PDMS, 2 μm embossed-PDMS and nano-embossed-PDMS films displayed water contact angles of approximately 106°, 125°, 125°, and 136°, respectively (Figure 4b). A relatively high water contact angle on the surface of dual-embossed-PDMS results from the increased air trap at the interface between the dual-embossed-PDMS with low surface energy and water droplets (i.e., because of the presence of hierarchical dual-

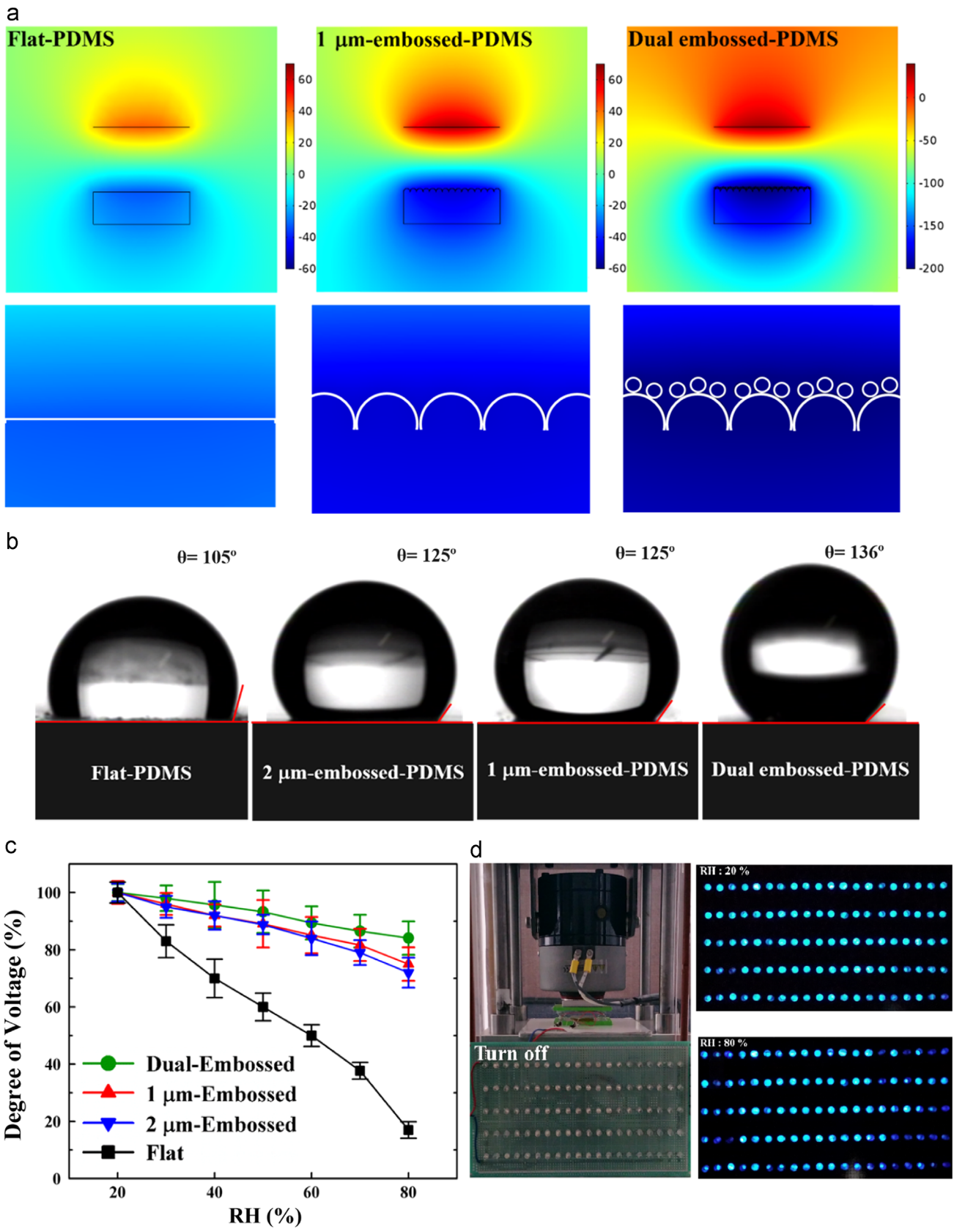

Figure 4 (a) Analytical (or color-coded) results showing triboelectric potential differences of flat, 1 μm-embossed and dual-embossed-PDMS films under the same compressive force, as simulated using the COMSOL multiphysics software. In this case, dual embossed-PDMS exhibited the largest potential differences. (b) Water contact angles on flat-TENG, 1 μm and 2 μm-embossed and dual-embossed-PDMS films. (c) The output voltages of flat TENG, 1 μm and 2 μm-embossed and dual-embossed-FTENGs as functions of RH. In these cases, a cycled compressive force of 90 N was used for the triboelectric measurements. The respective data points were the average values obtained from 100 cycles. (d) The use of electrical energy generated by the dual-embossed-FTENGs to operate 100 LEDs at 20% and 80% RH.

sized features and the inherently low surface energy of PDMS) [35]. This hydrophobicity can effectively screen the formation of a water moisture layer or at least minimize the contact area between water layer and PDMS surface because water droplet have much difficulty in being infiltrated into the air voids formed among the nano-sized protuberance with hydrophobic property. These phenomena can block a dramatic decrease in the triboelectric charging capacity by water moisture and is therefore helpful in maintaining stable performance under a high humid environment.

For confirming these possibilities, we investigated the change in output voltages of flat TENG, 1 μm embossed-FTENG, 2 μm embossed-FTENG and dual-embossed-FTENG as a function of relative humidity (RH%) (see Supporting Information, Figure S7 and Video S1). As shown in Figures 4c and S8, although the output voltages of all devices decreased because of the dissipation of triboelectric charges with increasing RH, the dual-embossed-FTENG displayed an output voltage of approximately 174 V at 80% RH, exhibiting only a 16% loss of the initial output voltage measured at 20% RH. By contrast, the output voltage of the flat TENG at 80% RH decreased from 73 to 11 V (i.e., approximately 85% loss) when the RH was increased from 20 to 80%. These results demonstrate that the electrical output of the dual-embossed-FTENG is less susceptible to humidity compared to other FTENGs based on flat or microstructured PDMS films. This lower susceptibility is a consequence of the surface of dual-embossed-PDMS, which imitates superhydrophobic surfaces, effectively preventing the formation of a water layer capable of dissipating the triboelectric charges or minimizing the contact area between water skin layer (or water droplet) and PDMS triboelectric film in a high humid environment [11]. Although triboelectric nanogenerators based on superhydrophobic PDMS films, despite successful preparation of PDMS films with real superhydrophobic surfaces (i.e., a water droplet contact angle $>150^{\circ}$) [43–45], have not been reported to date, our results suggest that the increase of hydrophobicity significantly minimizes the electrical performance loss of TENGs in high-humidity environments.

For the practical demonstration of the output power generation of the dual-embossed-FTENGs, we also designed a direct-current circuit composed of FTENGs and 100 commercial LEDs without a capacitor (Figures 4e, S9 and video S2). When the device at 20 and 80% RH was pushed once (with the force of 90 N) and then released, the 100 blue LEDs were instantaneously and simultaneously illuminated. However, the power delivered from flat TENGs under the same humidity conditions was not sufficient to turn on the 100 blue LEDs (see Supporting Information, Figure S10). These results demonstrate that the electric output performance of dual-embossed-FTENGs is less sensitive to humidity and that these devices therefore generate stable electrical output over a wide range of humidity conditions.

Supplementary material related to this article can be found online at http://dx.doi.org/10.1016/j.nanoen.2015.12.021.

Conclusions

We demonstrated that a large-area FTENG with a stable and high electrical output under high-humidity conditions could easily be prepared using a hierarchical surface-morphology-controlled triboelectric film. The electrical performance of FTENGs strongly depended on the structural shapes and the size of the morphological features that influenced the contact between the electrode and the triboelectric PDMS film. In particular, the output voltage and current density of dual-embossed-FTENG (under a compressive force of 90 N) were notably enhanced to 207 V and 141 mA m^{-2}, respectively, in contrast to those (73 V and 42 mA m^{-2}) of conventional TENGs composed of a flat PDMS film. In addition, the enhanced hydrophobicity of the dual-embossed-PDMS films, which imitate the micro/nanostructured morphology of a superhydrophobic surface, maintained triboelectric charges on the film surface for an extended period, which induced remarkably stable and high electrical performance under conditions of high humidity. Furthermore, these results suggest that the degradation of electrical performance of FTENGs under high-humidity conditions could be markedly minimized if real superhydrophobic surfaces with a water contact angle greater than 150° could be prepared by hierarchical surface-morphology-controlled triboelectric films with low surface energy. Our approach may provide a basis for designing and developing high-performance TENGs with highly humidity-resistant properties, large areas, and facile fabrication for the realization of self-powered electronics.

Acknowledgments

This work was supported by Samsung Research Funding Center of Samsung Electronics under Project Number SRFC-MA1301-07.

Appendix A. Supplementary material

Supplementary data associated with this article can be found in the online version at http://dx.doi.org/10.1016/j.nanoen.2015.12.021.

References

[1] Y. Qin, X.D. Wang, Z.L. Wang, Nature 451 (2008) 809–813.
[2] G.J. Snyder, E.S. Toberer, Nat. Mater. 7 (2008) 105–114.
[3] B. O'Regan, M. Grätzel, Nature 353 (1991) 737–740.
[4] Z.L. Wang, G. Zhu, Y. Yang, S. Wang, C. Pan, Mater. Today 15 (2012) 532–543.
[5] Z.L. Wang, W. Wu, Angew. Chem. Int. Ed. 51 (2012) 11700–11721.
[6]. S.-H. Kwon, J. Park, W.K. Kim, Y. Yang, E. Lee, C.J. Han, S. Y. Park, J. Lee, Y.S. Kim, Energy Env. Sci. 7 (2014) 3279–3283.
[7]. F.R. Fan, Z.Q. Tian, Z.L. Wang, Nano Energy 1 (2012) 328–334.
[8]. G. Zhu, C. Pan, W. Guo, C.Y. Chen, Y. Zhou, R. Yu, Z.L. Wang, Nano Lett. 12 (2012) 4960–4965.
[9]. S. Wang, Y. Xie, S. Niu, L. Lin, Z.L. Wang, Adv. Mater. 26 (2014) 2818–2824.
[10] S. Kim, M.K. Gupta, K.Y. Lee, A. Sohn, T.Y. Kim, K.-S. Shin, D. Kim, S.K. Kim, K.H. Lee, H.-J. Shin, D.-W. Kim, S.-W. Kim, Adv. Mater. 26 (2014) 3918–3925.
[11] K.Y. Lee, J. Chun, J.-H. Lee, K.N. Kim, N.-R. Kang, J.-Y. Kim, M.H. Kim, K.-S. Shin, M.K. Gupta, J.M. Baik, S.-W. Kim, Adv. Mater. 26 (2014) 5037–5042.

[12] C.K. Jeong, K.M. Baek, S. Niu, T.W. Nam, Y.H. Hur, D.Y. Park, G.-T. Hwang, M. Byun, Z.L. Wang, Y.S. Jung, K.J. Lee, Nano Lett. 14 (2014) 7031–7038.
[13] K.N. Kim, J. Chun, J.W. Kim, K.Y. Lee, J.-U. Park, S.-W. Kim, Z.L. Wang, J.M. Baik, ACS Nano 9 (2015) 6394–6400.
[14] X.-S. Zhang, M.-D. Han, R.-X. Wang, F.-Y. Zhu, Z.-H. Li, W. Wang, H.-X. Zhang, Nano Lett. 13 (2013) 1168–1172.
[15] H. Guo, J. Chen, L. Tian, Q. Leng, Y. Xi, C. Hu, ACS Appl. Mater. Interfaces 6 (2014) 17184–17189.
[16] J. Henniker, Nature 196 (1962) 474.
[17] A.F. Diaz, R.M. Felix-Navarro, J. Electrostat. 62 (2004) 277–290.
[18] Z.L. Wang, ACS Nano 7 (2013) 9533–9557.
[19] Y. Yang, H. Zhang, J. Chen, Q. Jing, Y.S. Zhou, X. Wen, Z.L. Wang, ACS Nano 7 (2013) 7342–7351.
[20] M. Taghavi, V. Mattoli, A. Sadeghi, B. Mazzolai, L. Beccai, Adv. Energy Mater. 4 (2014) 1400024.
[21] S. Wang, L. Lin, Z.L. Wang, Nano Lett. 12 (2012) 6339–6346.
[22] G. Zhu, Z.-H. Lin, Q. Jing, P. Bai, C. Pan, Y. Yang, Y. Zhou, Z.L. Wang, Nano Lett. 13 (2013) 847–853.
[23] L. Lin, S. Wang, Y. Xie, Q. Jing, S. Niu, Y. Hu, Z.L. Wang, Nano Lett. 13 (2013) 2916–2923.
[24] V. Albrecht, A. Janke, E. Németh, S. Spange, G. Schubert, F. Simon, J. Electrost. 67 (2009) 7–11.
[25] E. Németh, V. Albrecht, G. Schubert, F. Simon, J. Electrost. 58 (2003) 3–16.
[26] V. Nguyen, R. Zhu, R. Yang, Nano Energy 14 (2015) 49–61.
[27] V. Nguyen, R. Yang, Nano energy 2 (2013) 604–608.
[28] X.-S. Zhang, M.-D. Han, R.-X. Wang, B. Meng, F.-Y. Zhu, X.-M. Sun, W. Hu, W. Wang, Z.-H. Li, H.-X. Zhang, Nano Energy 4 (2014) 123–131.
[29] F.-R. Fan, L. Lin, G. Zhu, W. Wu, R. Zhang, Z.L. Wang, Nano Lett. 12 (2012) 3109–3114.
[30] Z.-H. Lin, G. Zhu, Y.S. Zhou, Y. Yang, P. Bai, J. Chen, Z.L. Wang, Angew. Chem. Int. Ed. 52 (2013) 5065–5069.
[31] A.S. Dimitrov, T. Miwa, K. Nagayama, Langmuir 15 (1999) 5257–5264.
[32] R.K. Idler, J. Colloid Interface Sci. 38 (1972) 496–501.
[33] C. Park., T. Lee, Y. Xia, T.J. Shin, J. Myoung, U. Jeong, Adv. Mater. 26 (2014) 4633–4638.
[34] S. Wang, L. Lin, Y. Xie, Q. Jing, S. Niu, Z.L. Wang, Nano Lett. 13 (2013) 2226–2233.
[35] A.B.D. Cassie, S. Bexter, Trans. Faraday Soc. 40 (1944) 546–551.
[36] R. Blossey, Nat. Mater. 2 (2003) 301–306.
[37] J. Hong, W. Bae, S. Oh, H. Lee, K. Char, F. Caruso, J. Cho, Adv. Mater. 19 (2007) 4364–4369.
[38] X. Hong, X. Gao, L. Jiang, J. Am. Chem. Soc. 129 (2007) 1478–1479.
[39] L. Zhang, J. Wu, Y. Wang, Y. Long, N. Zhao, J. Xu, J. Am. Chem. Soc. 134 (2012) 9879–9881.
[40] T. Darmanin, F. Guittard, J. Am. Chem. Soc. 133 (2011) 15627–15634.
[41] C. Zhang, W. Tang, C. Han, F. Fan, Z.L. Wang, Adv. Mater. 26 (2014) 3580–3591.
[42] S. Niu, S. Wang, L. Lin, Y. Liu, Y.S. Zhou, Y. Hu, Z.L. Wang, Energy Env. Sci. 6 (2013) 3576–3583.
[43] B. Cortese, S. D'Amone, M. Manca, I. Viola, R. Cingolani, G. Gigli, Langmuir 24 (2008) 2712–2718.
[44] M. Manca, B. Cortese, I. Viola, A.S. Arico, R. Cingolani, G. Gigli, Langmuir 24 (2008) 1833–1843.
[45] G. Davaasuren, C.-V. Ngo, H.-S. Oh, D.-M. Chun, Appl. Surf. Sci. 314 (2014) 530–536.

Dongjin Jang is a M.S. candidate under Prof. Jinhan Cho at Department of Chemical and Biological Engineering in Korea University. Currently, his research interest has focused on fabrication of various patterned-PDMS replicas and their device applications for energy harvesting.

Younghoon Kim is a postdoctoral researcher at the Department of Electrical and Computer Engineering in University of Toronto. He received his doctorate from the Department of Chemical and Biological Engineering in Korea University, Korea. His research has focused on the synthesis of functional nanocrystals in the range from metal, semiconducting to ceramics, the fabrication of nanocrystal-based thin films using layer-by-layer assembly, and their device applications for energy harvesting.

Tae Yun Kim is a Ph.D. candidate under Prof. Sang-Woo Kim at Advanced Materials Science & Engineering at Sungkyunkwan University (SKKU). His research interest has focused on FEM simulation of piezoelectric and triboelectric generator.

Kunsuk Koh is a M.S. candidate under Prof. Unyong Jeong at Department of Material Science and Engineering in Pohang University of Science and Technology (POSTECH). His Current research area is dry rubbing process for particle position registry.

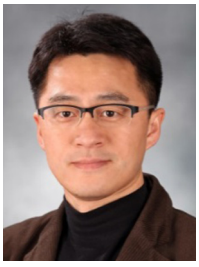

Unyong Jeong received a Ph.D. degree on polymer physics in chemical engineering from Pohang University of Science and Technology (POSTECH) in Korea (2003). After he studied the synthesis of inorganic nanomaterials during his post-doc period, he joined in Yonsei University in Korea (2006). He recently moved to MSE department at POSTECH (2015). His research aims at fabricating stretchable electronic devices based on material synthesis, assembly of nanomaterials, and formation of nanocomposites.

Jinhan Cho is a professor at the Department of Chemical & Biological Engineering in Korea University. Dr. Cho has expertize in the surface modification of metal or metal oxide nanoparticles as well as the layer-by-layer (LbL) assembled functional multilayers including optical films, nonvolatile memory devices, electrochemical sensors, energy harvesting/storage devices. He has focused on studying surface chemistry and electrochemical properties of various electrode materials, such as carbon nanotubes, graphenes, conducting polymers, and metal (or metal oxide) nanoparticles.